



Optics Letters

Deuterated silicon dioxide for heterogeneous integration of ultra-low-loss waveguides

WARREN JIN,^{1,*} DEMIS D. JOHN,¹ JARED F. BAUTERS,² TONY BOSCH,¹
BRIAN J. THIBEALT,¹ AND JOHN E. BOWERS¹

¹Electrical and Computer Engineering Department, University of California, Santa Barbara, California 93106, USA

²Juniper Networks, Inc., Goleta, California 93117, USA

*Corresponding author: warren@ece.ucsb.edu

Received 1 April 2020; revised 1 May 2020; accepted 1 May 2020; posted 1 May 2020 (Doc. ID 394121); published 15 June 2020

Ultra-low-loss waveguide fabrication typically requires high-temperature annealing beyond 1000°C to reduce the hydrogen content in deposited dielectric films. However, realizing the full potential of an ultra-low loss will require the integration of active materials that cannot tolerate high temperature. Uniting ultra-low-loss waveguides with on-chip sources, modulators, and detectors will require a low-temperature, low-loss dielectric to serve as a passivation and spacer layers for complex fabrication processes. We report a 250°C deuterated silicon dioxide film for top cladding in ultra-low-loss waveguides. Using multiple techniques, we measure propagation loss below 12 dB/m for the entire 1200–1650 nm range and top-cladding material absorption below 1 dB/m in the S, C, and L bands. © 2020 Optical Society of America

<https://doi.org/10.1364/OL.394121>

Recent advances in ultra-low-loss (<10 dB/m) waveguide technology have enabled photonic integrated circuit (PIC) demonstrations in a variety of applications, typically in the domain of fiber and bulk optics, including narrow linewidth lasers [1–4], optical gyroscopes [5,6], and nonlinear optical frequency conversion [7,8]. However, the majority of ultra-low-loss devices require co-packaging with fiber [9] or active PICs [3,4,10], since integration of on-chip light sources is highly challenging. To the best of our knowledge, the only technology capable of providing electrically pumped light generation and detection to ultra-low-loss devices on a single chip is heterogeneous integration of III–V semiconductor gain media [2,11].

Through heterogeneous integration, active material is bonded above the passive waveguide so that light may couple vertically between active and passive layers. After the active material has been bonded, a strict thermal budget must be imposed for all following process steps, otherwise the coefficient of the thermal expansion mismatch with the substrate will cause proliferation of the material defects in the gain medium [12,13]. However, as shown in Fig. 1, any additional passivation or spacer dielectrics for electrical routing will become upper cladding for the low-loss waveguide, and must therefore exhibit low loss

without the high-temperature annealing typically required to reduce hydrogen content [14,15]. This barrier to heterogeneous integration is especially severe for high-aspect-ratio waveguides in which the optical mode is squeezed into the cladding to achieve losses below 1 dB/m [1,16]. To integrate gain media with such devices without degrading performance, a low-loss, low-temperature deposited oxide cladding is required.

This problem is also relevant to the nonlinear integrated photonics community. As the field moves beyond the well-studied silicon nitride waveguide, promising new nonlinear platforms have emerged, which require low-loss top cladding but cannot tolerate high-temperature annealing. These include LiNbO₃ [8], AlGaAs [17], and GaP [18] on insulator, all formed by direct wafer bonding. It also includes Ta₂O₅ [19], which undergoes a phase change at 650°C. Furthermore, for integrated atomic clock applications, probing atomic resonances around 700 nm by frequency doubling will require eliminating the SiO–H absorption at 1390 nm.

In this work, we explore plasma-enhanced chemical vapor deposited (PECVD) SiO₂ films from a deuterated silane (SiD₄) precursor. We choose the PECVD technique due to its ability to provide high-quality, conformal silicon dioxide films at a low deposition temperature, as opposed to other chemical vapor deposition (CVD) techniques that require high temperature, or wafer bonding [16], which requires a planarized surface and so cannot provide a conformal coating. The main impact of the isotopic substitution of deuterium for hydrogen in the PECVD film is to shift the fundamental SiO–H absorption from its peak value at 2.73 μm to 3.74 μm, as shown in Fig. 2. In the near infrared, the corresponding first overtone of this absorption shifts from 1390 nm to 1870 nm, reducing the material loss in the technologically important C and O telecommunications bands. A summary of known hydrogen-induced absorption peaks in SiO₂:H and their corresponding locations in SiO₂:D can be found in Ref. [20]. While deuteration has been used to deposit PECVD silicon nitride [21,22] and to suppress O–H losses in optical fibers [20,23], deuterated silicon dioxide (SiO₂:D) has yet to be thoroughly explored in the context of integrated photonics.

We employ a silicon nitride waveguide with a 90 nm thick and 2.8 μm wide core, which is single mode in the C band.

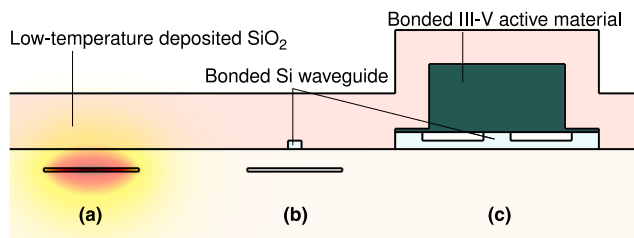


Fig. 1. Diagram of the heterogeneous integration approach in Ref. [11] for the waveguide geometry used in this Letter: (a) ultra-low-loss waveguide with its optical mode profile overlaid, (b) silicon to ultra-low-loss transition, and (c) hybrid silicon/III-V active waveguide. Low temperature oxide, indicated above, is necessary for passivation and electrical routing after III-V material has been bonded. It must also have low optical loss, as it overlaps the mode of the ultra-low-loss waveguide at (a).

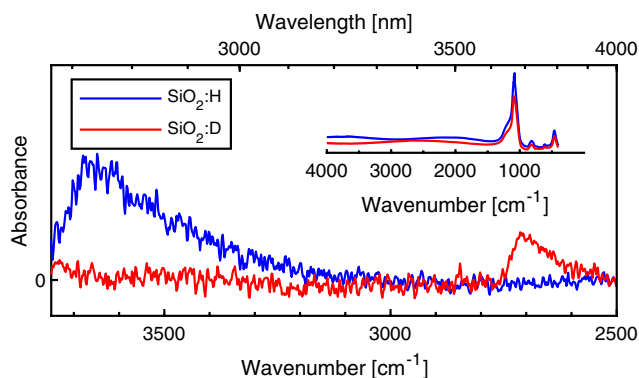


Fig. 2. Absorbance of SiO₂:H and SiO₂:D thin films by Fourier-transform infrared (FTIR) spectroscopy. The fundamental SiO–H vibrational mode at 2.73 μm shifts to 3.74 μm for SiO–D. The full FTIR spectrum is shown in the inset. A model of the Fabry–Perot ripple was fitted over 2500 to 4000 cm^{-1} and subtracted to reveal the absorption spectra of the fundamental vibrational modes of SiO–H and SiO–D, as shown above.

Due to the high-aspect-ratio design, the mode [shown in Fig. 1(a)] has a large overlap with the cladding and low impact of sidewall roughness allowing for a loss as low as 1 dB/m [14]—ideal for probing the intrinsic material loss limit of the SiO₂:D top cladding. We note that to measure the loss of the low-temperature top cladding, high-temperature processes are used to prepare a low-loss lower cladding and core. To prepare the samples, 90 nm of stoichiometric Si₃N₄ is deposited via a low-pressure chemical vapor deposition from dichlorosilane and ammonia precursors on 15 μm of thermal silicon dioxide at 800°C. The silicon nitride layer is patterned using 248 nm deep UV lithography and an inductively coupled plasma (ICP) etching in CHF₃/CF₄/O₂ gas. Prior to the top cladding deposition, the samples are annealed at 1050°C for 7 h. We measured that this reduces the residual SiN–H overtone at 1520 nm from over 50 dB/m to about 1 dB/m. Finally, the low-temperature top cladding is deposited to a thickness of at least 1.5 μm by an inductively coupled plasma chemical vapor deposition. The deposition parameters were 5 sccm SiH₄, 15 sccm O₂, 800 W ICP power, 0 W radio-frequency (RF) bias power, 5 mTorr chamber pressure, and 250°C temperature.

This recipe produces a film with a refractive index of 1.459 at a 632.8 wavelength nm and 1.451 at a 1550 nm wavelength, as measured by ellipsometry. After depositions with SiH₄ were complete, the line was evacuated and swapped to a SiD₄ gas cylinder with a 99% isotopic enrichment, and depositions were carried out with the same recipe parameters. The silane mass flow controller was not recalibrated after switching to SiD₄, as film parameters such as buffered oxide etch rate and refractive index were observed to be insensitive to minor changes in the gas flow. Devices in the following configurations were prepared: (1) a 2.8 μm wide waveguide with a SiH₄-based top cladding, and a length of either 0.8 cm or 0.5 m; (2) a 2.8 μm wide waveguide with a SiD₄-based top cladding, and a length of 3 m; and (3) whispering-gallery ring resonators with a SiD₄-based top cladding designed with long, phase-matched pulley couplers [24], as shown in Fig. 3(c), for selective coupling to the fundamental mode in either the C band or the O band. All the devices were laid out with at least a 1 mm bend radius to ensure a negligible bend loss.

Finally, samples were diced into chips and tested by edge coupling using a cleaved fiber and index-matching gel with a coupling loss of approximately 3 dB per facet. In order to measure the waveguide loss, multiple techniques, each with unique benefits and drawbacks, were used to probe the loss at various wavelengths. By comparing them, we were able to obtain loss estimates with high accuracy and spectral resolution.

- Optical frequency domain reflectometry (OFDR) (Luna OBR 4400 and 4413) was used to measure a propagation loss over 1525 nm to 1610 nm and 1280 nm to 1340 nm. Spectral

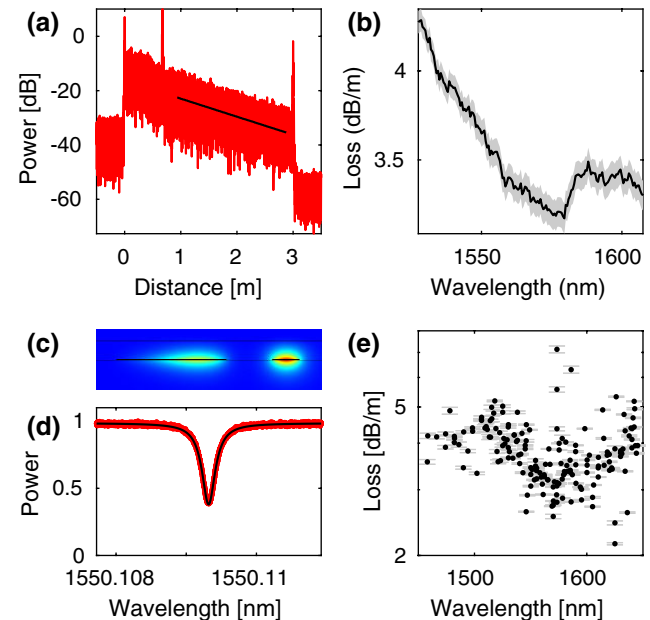


Fig. 3. Overview of OFDR and resonator loss measurement techniques. (a) Fitting the slope of the backscattered OFDR signal as a function of distance allows for (b) the measurement of the waveguide loss as a function of the wavelength. For the 2 m segment analyzed in (a), the fitting generates a 95% confidence interval (CI) of ± 0.07 dB/m indicated by the shaded area in (b). Through design of (c) resonator and coupler mode, and (d) fitting the optical linewidth, we demonstrate (e) robust fitting of multiple resonance spectra to measure spectral dependence of propagation loss, with mean 95% CI of ± 0.025 dB/m.

data was obtained by analyzing the backscatter signal in 5 nm windows at 0.5 nm increments, as shown in Figs. 3(a) and 3(b). OFDR provides an accurate measurement of propagation loss that is independent of the coupling loss to the chip, however precision is proportional to the propagation distance and can require prohibitively long lengths due to the stochastic nature of the distributed backscatter.

- The ring resonator linewidth was measured using a tunable laser (Keysight 81608A) and photodetector over 1240 nm to 1380 nm and 1450 nm to 1650 nm. By fitting the lineshape of under-coupled ring resonators, accurate measures of propagation loss could be obtained in wavelength ranges where OFDR was not available. As shown in Figs. 3(d) and 3(e), the uncertainty introduced by fitting is negligible. Instead, the precision of the measurement was limited by the phase noise of the laser, which caused a jitter in the tuning rate. This source of noise can be addressed by simultaneous use of an interferometer to correct the tuning rate [9].

- Tunable laser (TL) (Keysight 81608A) transmission spectrum over 1240 nm to 1380 nm and 1450 nm to 1650 nm was able to resolve fine spectral features. However, due to uncertainty in the coupling loss, it was necessary to reference this data to more accurate measurements such as OFDR and ring resonator linewidth. The broadband spectral dependence of the coupling loss also distorts the data.

- Superluminescent diode (SLED) transmission spectra, spanning from 1200 nm to 1700 nm and measured with an optical spectrum analyzer (OSA) (Yokogawa AQ6370C), provided broadband estimates of waveguide loss. However, the difficulty of obtaining consistent coupling to the chip over a broad wavelength span, as well as environmental perturbations due to the long scanning duration required to improve OSA sensitivity, led to severe uncertainty in coupling loss to the chip, in particular, a large spectral variability of the coupling loss. As such, while the spectra produced by this method provide qualitative insight into resonance wavelength and magnitude, the accuracy is poor when fiber-to-chip coupling losses greatly exceed accumulated propagation loss within the waveguide. This problem is more acute in spectral windows where the propagation loss is low.

The data obtained by these techniques is summarized for the SiO₂:H top cladding in Fig. 4 and the SiO₂:D top cladding in Fig. 5, with a comparison of the two in Fig. 4. In particular, we observe that the loss from the SiO–H overtone at 1390 nm is 30 times lower, reduced from 300 dB/m to 10 dB/m. We attribute the residual absorption at this wavelength to isotopic impurity of the source and trace H₂O contamination within the chamber. Regarding the other absorption features, deuteration shifts the 1240 nm SiO₂:H resonance, which is visible in Fig. 4, to 1680 nm [20], the tail of which is visible in Fig. 5. The SiO₂:H absorption lines at 950 nm and 1130 nm are shifted to 1270 nm and 1580 nm following deuteration [20], as observed in Fig. 5. Common to both Fig. 4 and Fig. 5 is the residual 1520 nm SiN–H overtone absorption [21,22] due to the waveguide core.

To infer the relative contributions of scattering loss and material absorption loss, we fit an approximate model to the data in Fig. 5. We adopt a scattering loss model $\alpha_{sc} \propto 1/\lambda^p$, where α_{sc} is the scattering component of the propagation loss, λ is the wavelength, and p is a fitted parameter. Based on analytical scattering models, we expect $p \approx 4$ [14]. In addition, we also fit a Lorentzian distribution to each of the absorption peaks around 1270 nm, 1390 nm, 1520 nm, 1580 nm, and 1680 nm.

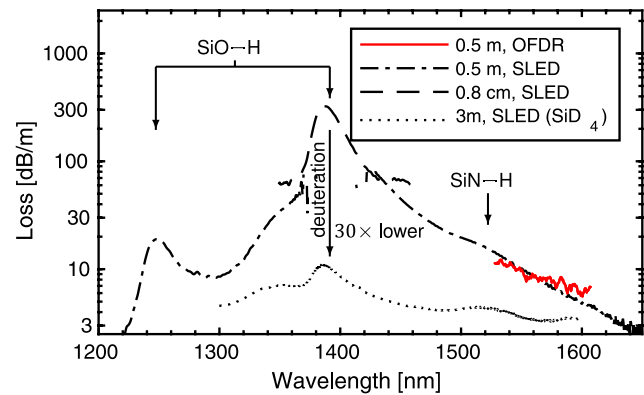


Fig. 4. Waveguide loss with a top cladding from the SiH₄ precursor. Uniform offsets were applied to the SLED transmission spectra to obtain approximate agreement with OFDR-measured loss in the C band. We also show the loss from the SiD₄ precursor (reproduced from Fig. 5) to demonstrate a 30× reduction at the 1390 nm peak.

As the O–H absorption feature in reality consists of multiple overlapping vibrational modes [25], a Lorentzian fit to a single line has limited accuracy. Nonetheless, an adequate fit to the data was obtained, as shown in Fig. 6. We conclude that in the transmission windows 1310 nm to 1360 nm and 1440 nm to 1630 nm, the majority of propagation loss is due to scattering, with material absorption contributing below 1 dB/m. We note that the 1520 nm peak contributing approximately 1 dB/m is associated with the core, rather than the top cladding. Furthermore, as shown in Fig. 5, the loss measured by OFDR in a single-mode waveguide (2.8 μm width) agrees closely with the loss extracted from resonance fitting of whispering gallery mode resonators (12 μm width). Since a sidewall scattering loss typically falls with an increasing waveguide width [26], we conclude that sidewall scattering is negligible and that the scattering loss is mostly due to roughness at the top surface of the waveguide core ($R_q = 0.4$ nm).

As the field of integrated photonics matures, it will move beyond the communications O, S, C, and L wavelength bands studied in this Letter. In particular, the visible and near-visible wavelength ranges of 0.4 μm to 1.0 μm will be of interest for

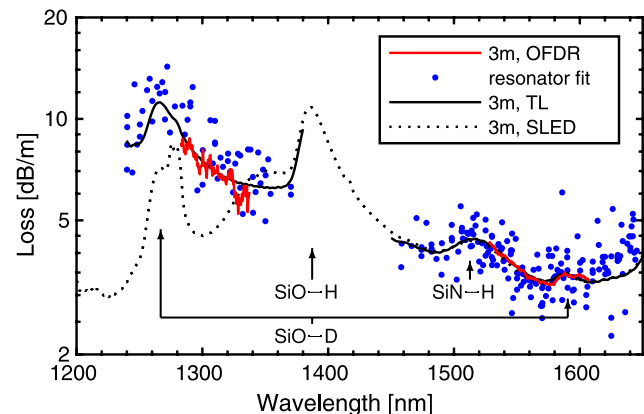


Fig. 5. Waveguide loss with top cladding from SiD₄ precursor. Uniform offsets were applied to the SLED and TL transmission spectra to obtain an approximate agreement with OFDR and ring resonator data in the C and O bands.

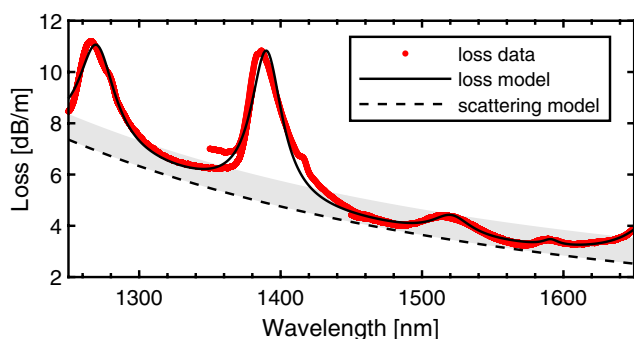


Fig. 6. Simple model including scattering and material losses was fitted to data from Fig. 5 for waveguides with deuterated top cladding. The region above the scattering model has been shaded to indicate where the material loss is below 1 dB/m. The scattering loss follows a $1/\lambda^p$ dependence where $p = 3.86 \pm 0.04$, while each absorption is approximately modeled by a Lorentzian resonance (95%CI, $R^2 = 0.99$).

applications involving quantum information [27] and frequency stabilization to atomic resonances [28]. Nonetheless, we believe that the low-temperature, low-loss cladding material developed in this Letter will prove critical to heterogeneous integration of frequency-doubling-based approaches [28], as such systems will still require ultra-low loss in the near infrared. However, we expect that deuteration will provide a reduced benefit to propagation loss in the near-visible, since O–H absorption bands in this spectral range correspond to the orders-of-magnitude weaker fourth and fifth harmonic overtones of the O–H bond resonances, rather than the second and third harmonic overtones in the near infrared [20,29]. Rather, we expect losses in this range to be dominated by scattering losses due to the $1/\lambda^4$ dependence of scattering loss on the wavelength, as discussed above.

In conclusion, we have demonstrated a high-quality 250°C SiO₂ film for use as top cladding in ultra-low-loss waveguides. In high-aspect-ratio silicon nitride, we measured a total propagation loss below 5 dB/m and a material absorption loss below 1 dB/m across the entire S, C, and L bands without annealing after top cladding deposition. We believe this approach will be critical for integration of active III–V material with ultra-low-loss waveguides and other platforms with limited thermal budget, thereby enabling a new generation of compact, all-on-chip narrow linewidth lasers, sensors, and nonlinear devices.

Funding. Defense Advanced Research Project Agency (W911NF-19-C-0003); National Science Foundation (DMR 1720256).

Acknowledgment. We thank Renan Moreira at UCSB, and Jeff Chiles and Nima Nader at NIST for helpful discussions. We thank Tom Reynolds at the UCSB Nanofabrication Facility for helping to maintain the ICPCVD tool. We thank Jaya Nolt at UCSB MRL for FTIR measurements. The MRL Shared Experimental Facilities are supported by the MRSEC Program of the NSF, a member of the NSF-funded Materials Research Facilities Network (www.mrfn.org).

Disclosures. The authors declare no conflicts of interest.

REFERENCES

- S. Gundavarapu, G. M. Brodnik, M. Puckett, T. Huffman, D. Bose, R. Behunin, J. Wu, T. Qiu, C. Pinho, N. Chauhan, J. Nohava, P. T. Rakich, K. D. Nelson, M. Salit, and D. J. Blumenthal, *Nat. Photonics* **13**, 60 (2019).
- D. Huang, M. A. Tran, J. Guo, J. Peters, T. Komljenovic, A. Malik, P. A. Morton, and J. E. Bowers, *Optica* **6**, 745 (2019).
- C. Xiang, P. A. Morton, and J. E. Bowers, *Opt. Lett.* **44**, 3825 (2019).
- Y. Fan, A. van Rees, P. J. van der Slot, J. Mak, R. Oldenbeuving, M. Hoekman, D. Gekus, C. G. Roeloffzen, and K.-J. Boller, "Ultra-narrow linewidth hybrid integrated semiconductor laser," arXiv:1910.08141 (2019).
- Y.-H. Lai, M.-G. Suh, Y.-K. Lu, B. Shen, Q.-F. Yang, H. Wang, J. Li, S. H. Lee, K. Y. Yang, and K. Vahala, *Nat. Photonics* **14**, 345 (2020).
- S. Gundavarapu, M. Belt, T. A. Huffman, M. A. Tran, T. Komljenovic, J. E. Bowers, and D. J. Blumenthal, *J. Lightwave Technol.* **36**, 1185 (2018).
- T. J. Kippenberg, A. L. Gaeta, M. Lipson, and M. L. Gorodetsky, *Science* **361**, eaan8083 (2018).
- M. Zhang, B. Buscaino, C. Wang, A. Shams-Ansari, C. Reimer, R. Zhu, J. M. Kahn, and M. Lončar, *Nature* **568**, 373 (2019).
- K. Y. Yang, D. Y. Oh, S. H. Lee, Q.-F. Yang, X. Yi, B. Shen, H. Wang, and K. Vahala, *Nat. Photonics* **12**, 297 (2018).
- B. Stern, X. Ji, Y. Okawachi, A. L. Gaeta, and M. Lipson, *Nature* **562**, 401 (2018).
- C. Xiang, W. Jin, J. Guo, J. D. Peters, M. Kennedy, J. Selvidge, P. A. Morton, and J. E. Bowers, *Optica* **7**, 20 (2020).
- T. Fujii, T. Sato, K. Takeda, K. Hasebe, T. Kakitsuka, and S. Matsuo, *IET Optoelectron.* **9**, 151 (2015).
- M. L. Davenport, "Heterogeneous silicon III-V mode-locked lasers," Ph.D. thesis (University of California, 2017).
- J. F. Bauters, M. J. Heck, D. John, D. Dai, M.-C. Tien, J. S. Barton, A. Leinse, R. G. Heideman, D. J. Blumenthal, and J. E. Bowers, *Opt. Express* **19**, 3163 (2011).
- M. H. Pfeiffer, J. Liu, A. S. Raja, T. Morais, B. Ghadiani, and T. J. Kippenberg, *Optica* **5**, 884 (2018).
- J. F. Bauters, M. J. Heck, D. D. John, J. S. Barton, C. M. Bruinink, A. Leinse, R. G. Heideman, D. J. Blumenthal, and J. E. Bowers, *Opt. Express* **19**, 24090 (2011).
- L. Chang, W. Xie, H. Shu, Q.-F. Yang, B. Shen, A. Boes, J. D. Peters, W. Jin, C. Xiang, S. Liu, G. Moille, S.-P. Yu, X. Wang, K. Srinivasan, S. B. Papp, K. Vahala, and J. E. Bowers, *Nat. Commun.* **11**, 1331 (2020).
- D. J. Wilson, K. Schneider, S. Hönl, M. Anderson, Y. Baumgartner, L. Czornomaz, T. J. Kippenberg, and P. Seidler, *Nat. Photonics* **14**, 57 (2020).
- S.-P. Yu, D. C. Cole, H. Jung, G. T. Moille, K. Srinivasan, and S. B. Papp, "Spontaneous pulse formation in edge-less photonic crystal resonators," arXiv:2002.12502 (2020).
- M. Nakahara, Y. Ohmori, and H. Itoh, *Electron. Lett.* **20**, 327 (1984).
- F. G. Johnson, O. S. King, J. V. Hryniewicz, L. G. Joneckis, S. T. Chu, and D. M. Gill, "Use of deuterated gases for the vapor deposition of thin films for low-loss optical devices and waveguides," U.S. patent 6,614,977 (2 September 2003).
- J. Chiles, N. Nader, D. D. Hickstein, S. P. Yu, T. C. Briles, D. Carlson, H. Jung, J. M. Shainline, S. Diddams, S. B. Papp, S. W. Nam, and R. P. Mirin, *Opt. Lett.* **43**, 1527 (2018).
- J. Stone, *J. Lightwave Technol.* **5**, 712 (1987).
- D. T. Spencer, J. F. Bauters, M. J. Heck, and J. E. Bowers, *Optica* **1**, 153 (2014).
- G. A. Thomas, B. I. Shraiman, P. F. Glodis, and M. J. Stephen, *Nature* **404**, 262 (2000).
- D. Marcuse, *Theory of Dielectric Optical Waveguides* (Academic, 1974).
- T. Chanellière, D. Matsukevich, S. Jenkins, S.-Y. Lan, T. Kennedy, and A. Kuzmich, *Nature* **438**, 833 (2005).
- W. Zhang, L. Stern, D. Carlson, D. Bopp, Z. Newman, S. Kang, J. Kitching, and S. B. Papp, *Laser Photon. Rev.* **14**, 1900293 (2020).
- P. Kaiser, A. Tynes, H. Astle, A. Pearson, W. French, R. Jaeger, and A. Cherin, *J. Opt. Soc. Am.* **63**, 1141 (1973).